Bulk Metallic Glass-like Scattering Signal in Small Metallic Nanoparticles

Vicky V. T. Doan-Nguyen,[†,△] Simon A. J. Kimber,[‡,△] Diego Pontoni,[‡] Danielle Reifsnyder Hickey,[§] Benjamin T. Diroll,[§] Xiaohao Yang,[∥] Marcel Miglierini,[⊥,#] Christopher B. Murray,[†,§] and Simon J. L. Billinge[∥,⊗,*]

[†]Department of Materials Science and Engineering, University of Pennsylvania, Philadelphia, Pennsylvania 19104, United States, [‡]European Synchrotron Radiation Facility (ESRF), Grenoble Cedex 9, 38043, France, [§]Department of Chemistry, University of Pennsylvania, Philadelphia, Pennsylvania 19104, United States, [∥]Department of Applied Physics and Applied Mathematics, Columbia University, New York 10027, United States, [⊥]Faculty of Electrical Engineering and Information Technology, Institute of Nuclear and Physical Engineering, Slovak University of Technology, Ilkovičova 3, 81219 Bratislava, Slovakia, [#]RCATM, Palacky University, 17. Listopadu 12, 771 46 Olomouc, Czech Republic, and [⊗]Condensed Matter Physics and Materials Science Department, Brookhaven National Laboratory, Upton, New York 11973, United States. [△]V. V. T. Doan-Nguyen and S. A. J. Kimber contributed equally to this work.

ABSTRACT The atomic structure of Ni—Pd nanoparticles has been studied using atomic pair distribution function (PDF) analysis of X-ray total scattering data and with transmission electron microscopy (TEM). Larger nanoparticles have PDFs corresponding to the bulk face-centered cubic packing. However, the smallest nanoparticles have PDFs that strongly resemble those obtained from bulk metallic glasses (BMGs). In fact, by simply scaling the distance axis by the mean metallic radius, the curves may be collapsed onto each other and onto the PDF from a metallic glass sample. In common with a wide range of BMG materials, the intermediate range order may be fit with a damped single-frequency sine wave. When viewed in high-resolution TEM, these nanoparticles exhibit atomic fringes typical of those seen in small metallic clusters with icosahedral or decahedral order. These two seemingly contradictory results are reconciled by calculating the PDFs of models of icosahedra that would be consistent with the fringes seen in TEM. These model PDFs resemble the measured ones when significant atom-position disorder is introduced, drawing together the two diverse fields of metallic nanoparticles and BMGs and supporting the view that BMGs may contain significant icosahedral or decahedral order.

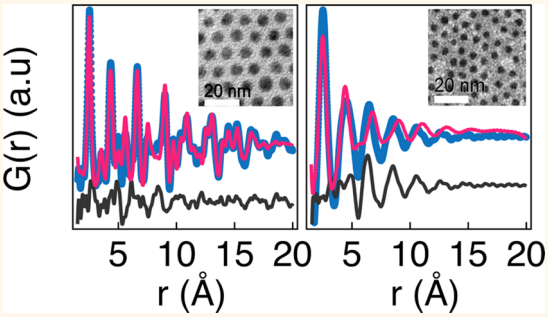

KEYWORDS: metal nanoparticles · total X-ray scattering · pair distribution functions · icosahedral atomic packing

The structure of small metallic nanoparticles has been the subject of extensive research for many years.[1−5] Although the boundary is somewhat blurred, such nanostructures have often been separated into clusters on one hand and colloidal nanoparticles (NPs) on the other. The former tend to be smaller and are often formed in atomic beam experiments,[6,7] whereas the latter are made using approaches such as arrested precipitation from a solvent and are capped with organic ligands that stabilize them.[8−12] Clusters may be separated into perfectly monodisperse samples, and it is meaningful to discuss the solution of their structure on the assumption that it is unique and well-defined. The structures of small metallic clusters have been extensively studied using transmission electron microscopy (TEM) with a prevalence of decahedral and icosahedral packing motifs.[13−15] Furthermore, through seeded or ripening growth mechanisms, larger NPs with the same platonic morphology have also been synthesized and characterized *via* electron microscopy.[16−24]

On the other hand, colloidal nanoparticles are made in bulk quantities, and samples have a range of structures and sizes for a library of technological applications.[25−31] Larger NPs take the structure of the parent material and resemble small chunks of the bulk parent, albeit with different defects.[32−35] However, at very small sizes, their structures may be modified qualitatively from the bulk,[36,37] with a tendency toward structural disorder. Some very stable small NPs form crystals of identical particles, and the structure may be refined by crystallographic methods. These are characterized by lower symmetry—even chiral—structures built around decahedral or icosahedral cores similar to those seen in the metallic clusters.[38−43] Nanoparticles that crystallize are the exception rather than

* Address correspondence to sb2896@columbia.edu.

Received for review March 21, 2014 and accepted May 28, 2014.

Published online May 28, 2014
10.1021/nn501591g

the rule, and it is important to develop methods to study the structure of small metallic NPs in general.[44]

Improvements in colloidal synthesis methods of metallic nanoparticles have resulted in bulk samples of very small particles that are highly monodisperse.[8] Concurrently, powerful new methods are emerging, such as the atomic pair distribution function (PDF) approach,[45] for characterizing the structure of small clusters and nanoparticles. Here we combine these developments in a study with synchrotron-based total X-ray scattering PDF methods applied to highly monodisperse Ni, Pd, and Ni_xPd_{1-x} NPs.

We find that, below a certain NP size, the scattering signal and the resulting PDF from these systems change from that of the bulk close-packed fcc structure to an amorphous scattering signal. Interestingly, the amorphous signal is nearly identical to that observed in bulk metallic glasses (BMGs) formed from highly tuned mixes of particular elements.[46,47] The PDFs of BMGs are very characteristic, with broad sinusoidal oscillations extending a significant range up to $r \approx 20$ Å,[48−50] and quite different from network glass PDFs, where the features disappear by $r = 10$ Å in general.[51,52] Given the isotropic, nonspecific, nature of the metallic bonding, and the extensive disorder coming from the BMG materials, the extent of the range of structural correlations is somewhat surprising. Furthermore, the presence of icosahedral-like packing in the BMGs has been studied using a combination of electron diffraction and X-ray scattering techniques.[53,54] It is striking that the ultrasmall nanoparticles studied here have a signal that can be mapped onto BMG signals with only a rescaling of the frequency and the phase of the sinusoidal signal. Additionally, the range of the oscillations and their damping envelope do not have to be rescaled. The frequency of the oscillations is rescaled by the mean metallic radius of the sample to bring the curves into agreement.

Quantitative nanoscale structure determination requires bulk probes that yield structural information on length scales below 10 nm. Recent developments of hard X-ray total scattering and atomic pair distribution function analysis have proven ideal for examining the structure of such nanoparticles.[55,56] PDF studies complement high-resolution transmission electron microscopy (HRTEM) experiments, which yield atomically resolved images of individual nanoparticles, by providing high-precision measurements of bond-length distributions and atomic arrangements averaged over the whole sample. Since the PDF is a sample average, the most precise structural information about individual nanoparticles requires samples that have great structure, size, and shape uniformity; otherwise sample polydispersity may limit the information available in the PDF. In cases where X-ray methods do not yield sufficient information to constrain a unique structural solution,[55] combining PDF data with complementary measurements such as HRTEM should be pursued.

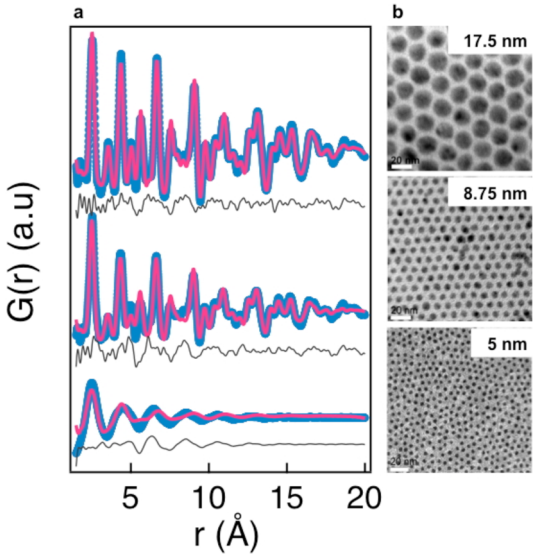

Figure 1. (A) Structural characterization of size-controlled nickel nanoparticles. Pair distribution functions for the three samples, as determined by Fourier transformation of high-energy X-ray scattering data. The blue points represent the data, and the red lines are fits of fcc-type models. The residuals of the fits are shown as black lines. (B) Transmission electron microscopy images of nickel nanoparticles. Note the formation of well-defined superlattices, which indicates uniformity. The scale bars correspond to 20 nm.

In the current study, we use nanoparticle samples prepared with precise control over size and shape uniformity, taking advantage of recent developments in metallic nanoparticle synthesis control. We characterize the particles by acquiring both high-quality PDF and HRTEM data. The uniformity of our samples is demonstrated by TEM images of Ni particles (Figure 1B). TEM images of the Pd and alloy samples exhibit similar uniformity. The PDF analysis was carried out on high-energy synchrotron X-ray data from size-selected Ni, Pd, and Ni_xPd_{1-x} alloy nanoparticles as a function of size and composition. HRTEM images were also collected for the smallest nanoparticles.

RESULTS

The PDF is the Fourier transform of the properly corrected and normalized total scattering powder diffraction intensity and may be understood as a histogram of the atomic distances in the material.[45] For example, the nearest neighbor distance in fcc nickel is 2.5 Å, corresponding to the first peak in the PDF. The PDFs of the larger particles show sharp peaks across a wide range of r as shown in Figure 1A. These could be modeled[57] using the fcc structure of bulk nickel modified by a spherical envelope function responsible for the falloff in PDF peak intensity with increasing r due to the finite particle size. However, this model fails to reproduce our data for the 5 nm particles. For the smallest particles, the PDF peaks are extremely broad, reflecting significant disorder. Even with extensive peak

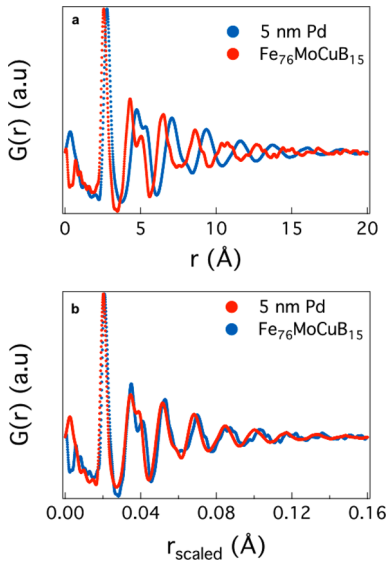

Figure 2. (A) Comparison of pair distribution functions of Pd nanoparticles and a representative bulk metallic glass, $Fe_{76}MoCuB_{15}$. Comparison of the pair distribution functions after correction for an overall scale factor. (B) Comparison of the pair distribution functions after scaling for the different metallic radii present in each sample.

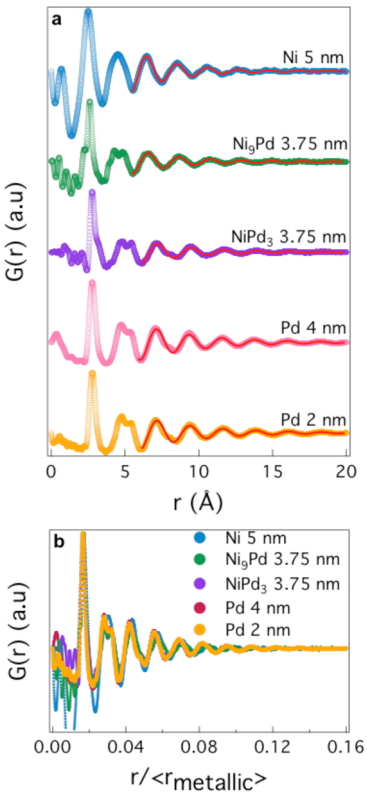

Figure 3. (A) Ubiquity of the disordered structure in the $Ni_{1-x}Pd_x$ solid solution series shown in pair distribution functions of the solid solutions. The red lines show fits to the high-*r* region of the PDF of a Gaussian-damped single-mode sine function as described in the text. (B) Comparison of the pair distribution functions after scaling by the different metallic radii in each sample.

broadening, the model peaks from the best-fit fcc model (continuous lines Figure 1A) are completely out-of-phase in the high-*r* region and clearly do not reproduce the measured PDF, which therefore is not simply describing disordered fcc local order: it is not possible to fit self-consistently with an fcc model both the low-*r* and high-*r* peaks in the PDF. Similar results were found in all small-sized (<5 nm) nanoparticles throughout the entire solid solution of Ni_xPd_{1-x} nanoparticles.

There is a striking resemblance between the PDFs of the small nanoparticles and those of bulk metallic glasses.[58−60] This is illustrated in Figure 2, which shows the PDF of a macroscopic ribbon of $Fe_{76}MoCuB_{15}$, plotted with the scattering from the small nanoparticles. The PDF of the ribbon is representative of a wide range of BMG samples and is used as a convenient reference for this class of materials.[61−67] In Figure 2A, the BMG PDF is overplotted by the PDF of 5 nm Pd nanoparticles with only a scale factor applied. The overall similarity of the curves is immediately apparent with broad sinusoidal features in both cases, although the phase and wavelength of the oscillations differ. However, a simple rescaling of the distance axis brings the two curves into correspondence. In Figure 2B we show the two curves plotted on top of each other after rescaling by the average metallic radius $\langle r_{metallic} \rangle$ of each sample. This simple scaling yields an agreement between the two data sets that is remarkable and superior to the best-fit fcc model. This is a strong indication that the nanoparticles, despite being made from elemental Ni, are mainly characterized by BMG-like disorder rather than a cubic-close-packed structure. While "disorder" has been observed in some small metallic nanoparticles, this close, quantitative, relationship to the BMG structure is heretofore unnoted.

The similarity between the nanoparticle and the rescaled BMG PDFs extends beyond peak positions and widths to the damping envelope, which is a measure of the range of structural coherence of the local order. The BMGs obtained from a wide range of compounds exhibit universal PDF features.[61,68] Our results extend such universality to simple-metal nanoparticles.

We now explore the ubiquity of this type of disordered structure for a range of small Ni, Pd, and $Ni_{1-x}Pd_x$ alloy nanoparticles. As shown in Figure 3A, the similarity of the intermediate range structure in all the samples is clearly apparent, with a broadened and non-fcc-like PDF above ~5 Å. This PDF can be well fit with a damped single-mode sine wave as shown in Figure 3A. This fact suggests that in this intermediate range the structure is isotropic, distinct from close-packed structures such as fcc and hcp that have different periodicities in the different crystallographic directions. In order to test whether all our samples show the same $\langle r_{metallic} \rangle$ scaling that we reported above, in Figure 3B we show all the rescaled curves plotted on top of each other. This simple scaling works remarkably well for all the Ni and alloy samples,

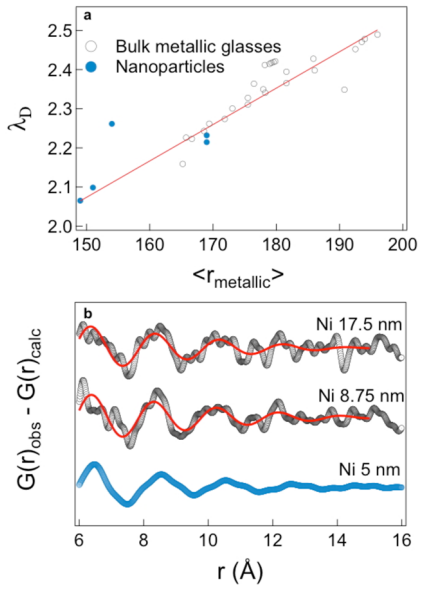

Figure 4. (A) Scaling of PDFs of synthesized NPs and bulk metallic glasses and evidence for a surface contribution in larger Ni particles. Linear dependence of the density wave fluctuations in NPs and BMGs on the average metallic radii. Data points were extracted using the fits shown in Figure 3A and from Ma *et al*. (B) Residuals from the fits of an fcc model to the data for larger Ni particles compared to the data for the 5 nm particles. Red lines show fits using a damped sine wave function as above.

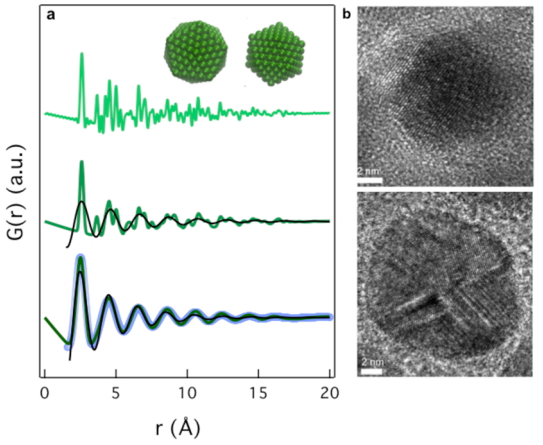

Figure 5. (A) PDFs of icosahedral models: Green curves are all PDFs from the 309-atom icosahedral model shown in the inset. In the top curve the PDF was calculated with an unrealistically small ADP of 0.001 Å^2. A more reasonable value for the ADP in the absence of static disorder is 0.01 Å^2, which is shown in the second curve from the top. The bottom green curve is the same model calculated with an ADP of 0.1 Å^2, which implies a considerable nonthermal distribution of atomic positions around the average site. The black curves are fits of a damped single-mode sine wave to the icosahedral PDFs. The underlying blue curve at the bottom is the measured PDF from the 5 nm Ni nanoparticles. In this case, the single-mode sine wave is the best-fit PDF of the same icosahedral model, where the only tunable parameters for refinement were a stretching parameter that allows the cluster to increase and decrease uniformly in diameter, a scale factor, and a single ADP parameter applied to all the atoms, plus a PDFgui "delta2" parameter that sharpens the PDF peaks in the low-*r* region. (B) High-resolution TEM images of 5 nm (top) and 17.7 nm (bottom) Ni nanoparticles show lattice fringes indicating the existence of twinning and local ordering within the nanostructures.

showing that the isotropic atomic packing is robust to a large variation in mean metallic radius. The agreement is still good, but less perfect, for the pure Pd nanoparticles.

The simple $\langle r_{metallic} \rangle$ scaling is different from the fractal scaling reported in Ma *et al*. and has a simpler explanation: that the packing is isotropic and depends only on the mean metallic radius for a wide range of BMGs.[69] Figure 4 shows that the new data from these NP experiments significantly extend the range of $\langle r_{metallic} \rangle$ over which the scaling analysis can be carried out, giving a more accurate determination of the exponent, if indeed it is valid to combine the NP and BMG signals.

Ultrasmall metallic clusters often form in cuboctahedral, decahedral, or icosahedral morphologies, as suggested by HRTEM measurements.[14] HRTEM images of the 5 nm clusters are shown in Figure 5b, top, where it is immediately clear that, despite the "glassy" PDF signal, lattice fringes are evident in the images, suggesting a well-defined short-range structure. By tilting the microscope stage appropriately it is possible to see lattice fringes in virtually all the particles, suggesting that this is not a minor effect affecting only a few particles. To reconcile these apparently contradictory HRTEM and PDF results, we calculated the PDFs of icosahedral clusters, which have well-defined order but are highly isotropic. The calculated PDFs for 309-atom icosahedra, which consist of a core atom surrounded by four additional atomic shells, are shown in Figure 5, with the icosahedral structure shown in the upper inset. The green curves are all PDFs calculated from this icosahedral model with different atomic displacement parameters (ADPs), which are a measure of the static and dynamic atomic disorder. The top curve has an unrealistically small ADP of 0.001 Å^2, but it serves to illustrate the large number of distinct atomic distances present in the perfect icosahedral cluster. The second green curve was calculated with an ADP of 0.01 Å^2, which is a reasonable value if there was just thermal motion but no static disorder in the material. The third green curve—overlaid on top of the 5 nm Ni PDF—was calculated with a large value of 0.1 Å^2. This is appropriate if there is a broad atomic positional distribution around the average sites in the icosahedral cluster. In the latter two cases a damped sine wave is shown overlaid in black. The good agreement shows that the PDF of a broadened icosahedral model is well represented by a damped single-mode sine wave, consistent with the measured PDF of the icosahedral clusters. Moreover, we have attempted fits of the icosahedral model to the nanoparticle PDFs where the only tunable structural parameters are an isotropic breathing parameter that allows the cluster to uniformly shrink or expand and a single global ADP. Additionally, the fits

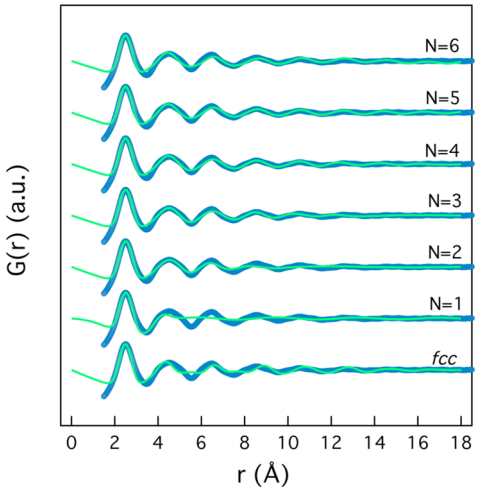

Figure 6. Calculated *G*(*r*) for icosahedral clusters increasing in the number of shells, thus increasing in size (blue). The curves of calculated PDFs of icosahedral clusters are overlaid with experimental total scattering data for 5 nm nanoparticles.

include a tunable scale factor and a correlation parameter that allows lower-*r* PDF peaks to be sharper, thus bringing to five the total number of fitting parameters. The results of the fit are shown as the bottom curve in Figure 5. The agreement between the fit and experimental data shows that a well-defined local icosahedral atomic geometry, albeit with a large atomic density distribution around each average atomic position, is consistent with the PDF data. We note that the PDF peaks are too broad and the nanoparticles too disordered to claim that the icosahedral model gives the "correct" packing arrangement. Other isotropic models such as decahedral might also be expected to give good agreement with the data after broadening. However, models such as cubic close packing that have different frequencies in different directions are not consistent with the data.

The fringes in the TEM survive presumably because the intermediate range order is well-defined. Even though the positional order of the atoms around each average atomic position is loose, the average position itself is well enough defined to yield interference and fringes in the HRTEM image. Furthermore, the disorder within the nanoparticle can be compared with calculated PDFs of bare icosahedral clusters ranging in size from 0.4 to 2.5 nm as seen in Figure 6. The corresponding number of shells for the icosahedral clusters has been tabulated in Table 1. The broadened *G*(*r*) curves for the clusters are overlaid with experimental Ni 5 nm data to demonstrate the consistency of the model.

DISCUSSION

The appearance of isotropic glassy packing consistent with non-space-filling packing of atoms below a critical diameter in Ni suggests that the vicinity of a surface may be important to stabilize it. Atomic

TABLE 1. Calculated Number of Atoms and Size of Icosahedral Clusters Ranging from 1 to 6 Shells

number of shells	number of atoms
1	13
2	55
3	147
4	309
5	561
6	923

arrangements routinely reconstruct at surfaces, and highly curved surfaces may result in reconstructions that appear quite disordered.[70,71] However, in these nanoparticles the structure of the core and the surface changes below a critical diameter, which is much larger than the first one or two atomic layers, but comparable to twice the range of coherence of the intermediate order. This means that the icosahedral cluster around any origin atom will not span the diameter of the particle, but is likely to impinge on a surface in some direction. We speculate that the large ADP values may arise from the need to create interpenetrating icosahedra, centered on different atoms and randomly oriented. In this picture the nanoparticles apparently prefer defective icosahedral packing to fcc order at these small sizes. We speculate that the alloying of elements with a large size distribution in BMGs may achieve a similar effect by packing mismatches that create voids and free volume in the system. This allows for the non-space-filling, such as icosahedral, packing to form, with small interstitial atoms filling the voids to lower the energy further. Such ideas are not new,[49,72] but this work gives direct experimental support to their validity.

The idea that the presence of a surface might stabilize the icosahedral state led us to explore the possibility that there is a thin layer of icosahedrally packed structure at the surface of the larger Ni nanoparticles. Close examination of the difference curves in Figure 1 indicates that after fitting the fcc model there is considerable signal left in the residual which, although noisy, appears to have an oscillatory nature. The difference curves are plotted in Figure 4B and compared to the PDF of the 5 nm Ni particles. The similarity is again striking, and the same Gaussian-damped single-mode sine wave fits the data well. These observations are highly suggestive of the existence of glassy isotropic packing also in the larger particles, which we speculate are at the surface.

CONCLUSION

In summary, we have shown that an isotropic, non-space-filling, structure such as icosahedral clusters, highly analogous to the structure of bulk metallic glasses, emerges in very small Ni and Pd nanoparticles. We show that this structure is consistent with the

presence of an average geometry of four- or five-shell icosahedral clusters with significant atomic smearing. The stabilization of this non-space-filling cluster in very small nanoparticles, in the presence of a nearby surface, suggests the importance of the presence of free volume in stabilizing the structure in the bulk. The likelihood of this type of layer on the surface of larger Ni particles has profound implications for catalysis employing supported nanoparticles, since heterogeneous catalysis is mediated by the surface.

METHODS

Nickel(II) acetylacetonate, palladium(II) acetylacetonate, oleylamine (70%), trioctylphosphine (97%), and 1-octadecene were purchased from Sigma-Aldrich. Synthesis of nanoparticles involves Schlenk-line techniques that utilize thermal decomposition of a metal-salt precursor in a flask with surfactants and a high-boiling solvent. The reactant amounts and reaction and purification conditions are detailed in SI Table 1. The nanoparticles were deposited on 300-mesh carbon-coated copper grids purchased from Electron Microscopy Sciences. TEM was done on a JEOL 1400 TEM with a LaB_6 filament, operating at 120 kV and equipped with an SC1000 ORIUS CCD camera and Digital Micrograph software. HRTEM was done on a JEOL 2010F TEM/STEM, equipped with a field emission gun (FEG), operating at 200 kV as well as the National Center for Electron Microscopy's Philips CM300FEG/UT TEM with an FEG and low spherical aberration (C_s = 0.60 mm), operating at 300 kV. For ICP-OES, the nanoparticle samples were digested in 69.4% HNO_3 for 24 h. The solutions were diluted to 0.7−7 ppm. The nickel and palladium calibration standards (0.1−500 ppm) were prepared by diluting from Sigma-Aldrich TraceCERT-grade stock solutions of nickel 1000 ppm and palladium 970 ppm. The measurements were done using a Spectro Genesis spectrometer. Small-angle X-ray scattering data were collected at Penn using a multi-angle X-ray scattering system with 1.54 Å X-ray wavelength with detector distances at 11 and 54 cm as well as at the ESRF at ID02 using 12.5 keV X-rays with detector distances at 1.5 and 10 m covering a q range of 0.5−0.001 $Å^{-1}$. Collection of the X-ray scattering data was done at the ESRF at ID15B using 87.8 keV X-rays (0.1412 Å) and a Mar345 detector. The raw images were integrated using Fit2D.[73] Background contributions from the 2 mm Kapton capillary tubes as well as Compton and fluorescence contributions were subtracted from the data. An in-house code "iPDF" written by S.A.J.K. was used to correct and Fourier transform the data into real space pair distribution functions. PDFgui was used to model the PDFs in the small-box approximation.[57] The PDFs of icosahedral clusters were calculated using SrFit, a program framework for not only calculating functions but also co-refining structures with multiple sets of characterization data and model inputs.[74]

Conflict of Interest: The authors declare no competing financial interest.

Acknowledgment. This work was primarily supported by the U.S. Department of Energy (DOE). Development of synthesis techniques for Ni and Pd samples was supported by ARPA-E Award Number DE-AR0000123. SAXS and HRTEM data collection was supported from the DOE, Office of Science, Office of Basic Energy Sciences (BES), Division of Materials Science and Engineering, under Award Number DE-SC0002158. HRTEM was also performed in part at NCEM, which is supported by the DOE, BES under Contract Number DE-AC02-05CH11231. We thank Chengyu Song for assistance at NCEM. The PDF data analysis and modeling was supported by Laboratory Directed Research and Development (LDRD) Program 12-007 (Complex Modeling) at the Brookhaven National Laboratory, which is supported by the DOE, BES under Award Number DE-AC02-98CH10886. We thank the University of Pennsylvania Nano-Bio Interface Center and MINATEC Exchange program under the U.S. National Science Foundation, Office of International Science and Engineering, Division of International Research Experience for Students Award Number 1130994 for funding the visit of VDN to Grenoble, France. D.R.H. acknowledges additional support from the NSF-IGERT graduate student fellowship (Grant DGE-0221664). The European Synchrotron Radiation Facility is acknowledged for access to instrumentation. M.M. acknowledges the grant No. CZ.1.07/2.3.00/20.0155 for support of the bulk metallic glass synthesis and characterization work.

Supporting Information Available: The Supporting Information includes detailed reaction conditions for nanoparticle synthesis, ICP measurement conditions, TEM images of Ni and Pd nanoparticles, and small-angle X-ray scattering data. This material is available free of charge *via* the Internet at http://pubs.acs.org.

REFERENCES AND NOTES

1. Daniel, M.-C.; Astruc, D. Gold Nanoparticles: Assembly, Supramolecular Chemistry, Quantum-Size-Related Properties, and Applications toward Biology, Catalysis, and Nanotechnology. *Chem. Rev.* **2004**, *104*, 293–346.
2. Murray, C. B.; Sun, S. H.; Doyle, H.; Betley, T. Monodisperse 3d Transition-Metal (Co, Ni, Fe) Nanoparticles and Their Assembly into Nanoparticle Superlattices. *MRS Bull.* **2001**, *26*, 985–991.
3. Sun, Y.; Xia, Y. Shape-Controlled Synthesis of Gold and Silver Nanoparticles. *Science* **2002**, *298*, 2176–2179.
4. Nikoobakht, B.; El-Sayed, M. A. Preparation and Growth Mechanism of Gold Nanorods (NRs) Using Seed-Mediated Growth Method. *Chem. Mater.* **2003**, *15*, 1957–1962.
5. Wang, X.; Zhuang, J.; Peng, Q.; Li, Y. A General Strategy for Nanocrystal Synthesis. *Nature* **2005**, *437*, 121–124.
6. Longo, E.; Cavalcante, L. S.; Volanti, D. P.; Gouveia, A. F.; Longo, V. M.; Varela, J. A.; Orlandi, M. O.; Andres, J. Direct *in-Situ* Observation of the Electron-Driven Synthesis of Ag Filaments on Alpha-Ag_2WO_4 Crystals. *Sci. Rep.* **2013**, *3*, 1676.
7. Simonsen, S. B.; Chorkendorff, I.; Dahl, S.; Skoglundh, M.; Sehested, J.; Helveg, S. Direct Observations of Oxygen-Induced Platinum Nanoparticle Ripening Studied by *in-Situ* TEM. *J. Am. Chem. Soc.* **2010**, *132*, 7968–7975.
8. Murray, C. B.; Norris, D. J.; Bawendi, M. G. Synthesis and Characterization of Nearly Monodisperse CdE (E=S, Se,Te) Semiconductor Nanocrystals. *J. Am. Chem. Soc.* **1993**, *115*, 8706–8715.
9. Murray, C. B.; Sun, S.; Gaschler, W.; Doyle, H.; Betley, T. A.; Kagan, C. R. Colloidal Synthesis of Nanocrystals and Nanocrystal Superlattices. *IBM J. Res. Dev.* **2001**, *45*, 47–56.
10. Kang, Y.; Murray, C. B. Synthesis and Electrocatalytic Properties of Cubic Mn-Pt Nanocrystals (Nanocubes). *J. Am. Chem. Soc.* **2010**, *132*, 7568–7569.
11. Masala, O.; Seshadri, R. Synthesis Routes for Large Volumes of Nanoparticles. *Annu. Rev. Mater. Res.* **2004**, *34*, 41–81.
12. Zhou, W.; Wu, J.; Yang, H. Highly Uniform Platinum Icosahedra Made by Hot Injection-Assisted GRAILS Method. *Nano Lett.* **2013**, *13*, 2870–2874.
13. Marks, L. D.; Howie, A. Multiply-Twinned Particles in Silver Catalysts. *Nature* **1981**, *282*, 196–198.
14. Marks, L. D. Experimental Studies of Small Particle Structures. *Rep. Prog. Phys.* **1994**, *603*, 603–649.
15. Velazquez-Salazar, J. J.; Esparza, R.; Mejia-Rosales, S. J.; Estrada-Salas, R.; Ponce, A.; Deepak, F. L.; Castro-Guerrero, C.; Jose-Yacaman, M. Experimental Evidence of Icosahedral and Decahedral Packing in One-Dimensional Nanostructures. *ACS Nano* **2011**, *5*, 6272–6278.
16. Zhang, Q.; Xie, J.; Yang, J.; Lee, J. Y. Monodisperse Icosahedral Ag, Au, and Pd Nanoparticles: Size Control Strategy and Superlattice Formation. *ACS Nano* **2009**, *3*, 139–148.

17. Lim, B.; Xiong, Y.; Xia, Y. A Water-Based Synthesis of Octahedral, Decahedral, and Icosahedral Pd Nanocrystals Supporting Information. *Angew. Chem., Int. Ed.* **2007**, *46*, 9279–9282.
18. Seo, D.; Yoo, C. I.; Chung, I. S.; Park, S. M.; Ryu, S.; Song, H. Shape Adjustment between Multiply Twinned and Single-Crystalline Polyhedral Gold Nanocrystals: Decahedra, Icosahedra, and Truncated Tetrahedra. *J. Phys. Chem. C* **2008**, *112*, 2469–2475.
19. Habas, S. E.; Lee, H.; Radmilovic, V.; Somorjai, G. A.; Yang, P. Shaping Binary Metal Nanocrystals through Epitaxial Seeded Growth. *Nat. Mater.* **2007**, *6*, 692–697.
20. Wiley, B.; Sun, Y.; Mayers, B.; Xia, Y. Shape-Controlled Synthesis of Metal Nanostructures: The Case of Silver. *Chem.—Eur. J.* **2005**, *11*, 454–463.
21. Tao, A. R.; Habas, S.; Yang, P. Shape Control of Colloidal Metal Nanocrystals. *Small* **2008**, *4*, 310–325.
22. Tian, N.; Zhou, Z.-Y.; Sun, S.-G.; Ding, Y.; Wang, Z. L. Synthesis of Tetrahexahedral Platinum Nanocrystals with High-Index Facets and High Electro-Oxidation Activity. *Science* **2007**, *316*, 732–735.
23. Sau, T. K.; Rogach, A. L. Nonspherical Noble Metal Nanoparticles: Colloid-Chemical Synthesis and Morphology Control. *Adv. Mater.* **2010**, *22*, 1781–1804.
24. Kim, F.; Connor, S.; Song, H.; Kuykendall, T.; Yang, P. Platonic Gold Nanocrystals. *Angew. Chem., Int. Ed.* **2004**, *43*, 3673–3677.
25. Urban, J. J.; Talapin, D. V.; Shevchenko, E. V.; Murray, C. B. Self-Assembly of PbTe Quantum Dots into Nanocrystal Superlattices and Glassy Films. *J. Am. Chem. Soc.* **2006**, *128*, 3248–3255.
26. Liu, Y.; Ko, D.; Oh, S. J.; Gordon, T. R.; Doan-Nguyen, V.; Paik, T.; Kang, Y.; Ye, X.; Jin, L.; Kagan, C. R.; *et al*. Near-Infrared Absorption of Monodisperse Silver Telluride (Ag_2Te) Nanocrystals and Photoconductive Response of Their Self-Assembled Superlattices. *Chem. Mater.* **2011**, *23*, 4657–4659.
27. Cargnello, M.; Doan-Nguyen, V. V. T.; Gordon, T. R.; Paik, T.; Diaz, R. E.; Stach, E. A.; Gorte, R. J.; Fornasiero, P.; Murray, C. B. Nanoscale Engineering of the Metal-Support Interface Reveals Its Crucial Role in Ceria-Based Catalysts. *Science* **2013**, *341*, 771–773.
28. Black, C. T.; Murray, C. B.; Sandstrom, R. L.; Sun, S. Spin-Dependent Tunneling in Self-Assembled Cobalt-Nanocrystal Superlattices. *Science* **2000**, *290*, 1131–1134.
29. Macfarlane, R. J.; Lee, B.; Jones, M. R.; Harris, N.; Schatz, G. C.; Mirkin, C. A. Nanoparticle Superlattice Engineering with DNA. *Science* **2011**, *334*, 204–208.
30. Chen, C.; Kang, Y.; Huo, Z.; Zhu, Z.; Huang, W.; Xin, H. L.; Snyder, J. D.; Li, D.; Herron, J. A.; Mavrikakis, M.; *et al*. Highly Crystalline Multimetallic Nanoframes with Three-Dimensional Electrocatalytic Surfaces. *Science* **2014**, *343*, 1339–1343.
31. Wu, J.; Qi, L.; You, H.; Gross, A.; Li, J.; Yang, H. Icosahedral Platinum Alloy Nanocrystals with Enhanced Electrocatalytic Activities. *J. Am. Chem. Soc.* **2012**, *134*, 11880–11883.
32. Neder, R. B.; Korsunskiy, V. I.; Chory, C.; Müller, G.; Hofmann, A.; Dembski, S.; Graf, C.; Rühl, E. Structural Characterization of II-VI Semiconductor Nanoparticles. *Phys. Status Solidi* **2007**, *4*, 3221–3233.
33. Masadeh, A. S.; Božin, E. S.; Farrow, C. L.; Paglia, G.; Juhas, P.; Billinge, S.; Karkamkar, A.; Kanatzidis, M. Quantitative Size-Dependent Structure and Strain Determination of CdSe Nanoparticles Using Atomic Pair Distribution Function Analysis. *Phys. Rev. B* **2007**, *76*, 115413.
34. Huang, W. J.; Sun, R.; Tao, J.; Menard, L. D.; Nuzzo, R. G.; Zuo, J. M. Coordination-Dependent Surface Atomic Contraction in Nanocrystals Revealed by Coherent Diffraction. *Nat. Mater.* **2008**, *7*, 308–313.
35. Page, K.; Hood, T. C.; Proffen, T.; Neder, R. B. Building and Refining Complete Nanoparticle Structures with Total Scattering Data. *J. Appl. Crystallogr.* **2011**, *44*, 327–336.
36. Rosenthal, S. J.; McBride, J. R.; Pennycook, S. J.; Feldman, L. C. Synthesis, Surface Studies, Composition and Structural Characterization of CdSe, Core/Shell and Biologically Active Nanocrystals. *Surf. Sci. Rep.* **2007**, *62*, 111–157.
37. Yang, X.; Masadeh, A.; McBride, J.; Bozin, E. S.; Rosenthal, S. J.; Billinge, S. J. L. Confirmation of Disordered Structure of Ultrasmall CdSe Nanoparticles from X-Ray Atomic Pair Distribution Function Analysis. *Phys. Chem. Chem. Phys.* **2013**, *15*, 8480.
38. Jadzinsky, P. D.; Calero, G.; Ackerson, C. J.; Bushnell, D. A.; Kornberg, R. D. Structure of a Thiol Monolayer-Protected Gold Nanoparticle at 1.1 A Resolution. *Science* **2007**, *318*, 430–433.
39. Zeng, C.; Li, T.; Das, A.; Rosi, N. L.; Jin, R. Chiral Structure of Thiolate-Protected 28-Gold-Atom Nanocluster Determined by X-Ray Crystallography. *J. Am. Chem. Soc.* **2013**, *135*, 10011–10013.
40. Frenkel, A. Solving the 3D Structure of Metal Nanoparticles. *Z. Kristallogr.* **2007**, *222*, 605–611.
41. Gafner, Y. Y.; Gafner, S. L.; Entel, P. Formation of an Icosahedral Structure during Crystallization of Nickel Nanoclusters. *Phys. Solid State* **2004**, *46*, 1327–1330.
42. Yi, X.; Liu, R.; Tian, Z.; Hou, Z.; Li, X.; Zhou, Q. Formation and Evolution Properties of Clusters in Liquid Metal Copper during Rapid Cooling Processes. *Trans. Nonferrous Met. Soc. China* **2008**, *18*, 33–39.
43. Barry, J. C.; Bursilla, A.; Sanders, J. V. Electron Microscope Images of Icosahedral and Cuboctahedral (f.c.c. Packing) Clusters of Atoms. *Aust. J. Phys.* **1985**, *38*, 437–448.
44. Chen, C.-C.; Zhu, C.; White, E. R.; Chiu, C.-Y.; Scott, M. C.; Regan, B. C.; Marks, L. D.; Huang, Y.; Miao, J. Three-Dimensional Imaging of Dislocations in a Nanoparticle at Atomic Resolution. *Nature* **2013**, *496*, 74–79.
45. Egami, T.; Billinge, S. J. L. *Underneath the Bragg Peaks: Structural Analysis of Complex Materials*, 2nd ed.; Elsevier: Amsterdam, 2013.
46. Peker, A.; Johnson, W. L. A Highly Processable Metallic Glass: Zr41.2Ti13.8Cu12.5Ni10.0Be22.5. *Appl. Phys. Lett.* **1993**, *63*, 2342.
47. Busch, R.; Kim, Y. J.; Johnson, W. L. Thermodynamics and Kinetics of the Undercooled Liquid and the Glass Transition of the Zr41.2Ti13.8Cu12.5Ni10.0Be22.5 Alloy. *J. Appl. Phys.* **1995**, *77*, 4039.
48. Voloshin, V. P.; Beaufils, S.; Medvedev, N. N. Void Space Analysis of the Structure of Liquids. *J. Mol. Liq.* **2002**, *96−97*, 101–112.
49. Voloshin, V. P.; Naberukhin, Y. I. On the Origin of the Splitting of the Second Maximum in the Radial Distribution Function of Amorphous Solids. *J. Struct. Chem.* **1997**, *38*, 62–70.
50. Chirawatkul, P.; Zeidler, A.; Salmon, P. S.; Takeda, S.; Kawakita, Y.; Usuki, T.; Fischer, H. E. Structure of Eutectic Liquids in the Au-Si, Au-Ge, and Ag-Ge Binary Systems by Neutron Diffraction. *Phys. Rev. B* **2011**, *83*, 014203.
51. Salmon, P. S.; Petri, I. Structure of Glassy and Liquid $GeSe_2$. *J. Phys.: Condens. Matter* **2003**, *15*, S1509–S1528.
52. Petkov, V.; Billinge, S.; Shastri, S.; Himmel, B. Polyhedral Units and Network Connectivity in Calcium Aluminosilicate Glasses from High-Energy X-Ray Diffraction. *Phys. Rev. Lett.* **2000**, *85*, 3436–3439.
53. Hirata, A.; Kang, L. J.; Fujita, T.; Klumov, B.; Matsue, K.; Kotani, M.; Yavari, A. R.; Chen, M. W. Geometric Frustration of Icosahedron in Metallic Glasses. *Science* **2013**, *341*, 376–379.
54. Di Cicco, A.; Trapananti, A.; Faggioni, S.; Filipponi, A. Is There Icosahedral Ordering in Liquid and Undercooled Metals? *Phys. Rev. Lett.* **2003**, *91*, 135505.
55. Billinge, S. J. L.; Levin, I. The Problem with Determining Atomic Structure at the Nanoscale. *Science* **2007**, *316*, 561–565.
56. Tyrsted, C.; Jensen, K. M. Ø.; Bøjesen, E. D.; Lock, N.; Christensen, M.; Billinge, S. J. L.; Brummerstedt Iversen, B. Understanding the Formation and Evolution of Ceria Nanoparticles under Hydrothermal Conditions. *Angew. Chem., Int. Ed.* **2012**, *51*, 9030–9033.
57. Farrow, C. L.; Juhas, P.; Liu, J. W.; Bryndin, D.; Bozin, E. S.; Bloch, J.; Proffen, T.; Billinge, S. J. L. PDFfit2 and PDFgui: Computer Programs for Studying Nanostructure in Crystals. *J. Phys.: Condens. Matter* **2007**, *19*, 335219.

58. Hwang, J.; Melgarejo, Z.; Kalay, Y.; Kalay, I.; Kramer, M.; Stone, D.; Voyles, P. Nanoscale Structure and Structural Relaxation in Zr50Cu45Al5 Bulk Metallic Glass. *Phys. Rev. Lett.* **2012**, *108*, 195505.
59. Miracle, D. B. A Structural Model for Metallic Glasses. *Nat. Mater.* **2004**, *3*, 697–702.
60. Hirata, A.; Guan, P.; Fujita, T.; Hirotsu, Y.; Inoue, A.; Yavari, A. R.; Sakurai, T.; Chen, M. Direct Observation of Local Atomic Order in a Metallic Glass. *Nat. Mater.* **2011**, *10*, 28–33.
61. Wang, W. H.; Dong, C.; Shek, C. H. Bulk Metallic Glasses. *Mater. Sci. Eng., R* **2004**, *44*, 45–89.
62. Liu, Y. H.; Wang, G.; Wang, R. J.; Zhao, D. Q.; Pan, M. X.; Wang, W. H. Super Plastic Bulk Metallic Glasses at Room Temperature. *Science* **2007**, *315*, 1385–1388.
63. Liu, X. J.; Xu, Y.; Lu, Z. P.; Hui, X.; Chen, G. L.; Zheng, G. P.; Liu, C. T. Atomic Packing Symmetry in the Metallic Liquid and Glass States. *Acta Mater.* **2011**, *59*, 6480–6488.
64. Basu, J.; Ranganathan, S. Bulk Metallic Glasses: A New Class of Engineering Materials. *Sadhana* **2003**, *28*, 783−798.
65. Hofmann, D. C.; Suh, J.-Y.; Wiest, A.; Duan, G.; Lind, M.-L.; Demetriou, M. D.; Johnson, W. L. Designing Metallic Glass Matrix Composites with High Toughness and Tensile Ductility. *Nature* **2008**, *451*, 1085–1089.
66. Klement, W.; Willens, R. H.; Duwez, P. Non-Crystalline Structure in Solidified Gold-Silicon Alloys. *Nature* **1960**, *187*, 869–870.
67. Duwez, P. Structure and Properties of Glassy Metals. *Annu. Rev.* **1976**, 83–117.
68. Schroers, J. Bulk Metallic Glasses. *Phys. Today* **2013**, *66*, 32.
69. Ma, D.; Stoica, A. D.; Wang, X. L. Power-Law Scaling and Fractal Nature of Medium-Range Order in Metallic Glasses. *Nat. Mater.* **2009**, *8*, 30–34.
70. Robinson, K.; Tweet, D. J. Surface X-Ray Diffraction. *Rep. Prog. Phys.* **1992**, *55*, 599–651.
71. Nam, H.-S.; Hwang, N.; Yu, B.; Yoon, J.-K. Formation of an Icosahedral Structure during the Freezing of Gold Nanoclusters: Surface-Induced Mechanism. *Phys. Rev. Lett.* **2002**, *89*, 275502.
72. Cheng, Y. Q.; Ma, E. Atomic-Level Structure and Structure−Property Relationship in Metallic Glasses. *Prog. Mater. Sci.* **2011**, *56*, 379–473.
73. Hammersley, A. P.; Svensson, S. O.; Hanfland, M.; Fitch, A. N.; Hausermann, D. Two-Dimensional Detector Software: From Real Detector to Idealised Image or Two-Theta Scan. *High Press. Res.* **1996**, *14*, 235–248.
74. Farrow, C.; Juhas, P.; Billinge, S. J. L. *SrFit*; http://www.diffpy.org/.